Elsevier Editorial System(tm) for Applied Energy
Manuscript Draft

Manuscript Number:

Title: Analysis and characterization of photovoltaic modules of three different thin-film technologies in outdoor conditions

Article Type: Original Paper

Keywords: thin film technologies; photovoltaic modules; performance ratio; contour graphs; outdoor conditions

Corresponding Author: Mrs. Llanos Mora-López, Ph.D.

Corresponding Author's Institution: University of Malaga

First Author: Rafael Moreno-Sáez, Ph.D.

Order of Authors: Rafael Moreno-Sáez, Ph.D.; Mariano Sidrach-de-Cardona, Ph.D.; Llanos Mora-López, Ph.D.

Abstract: The instantaneous performance ratio of thin-film photovoltaic modules of three different technologies is analyzed and characterized using contour graphs for different outdoor conditions. This parameter changes when modules are working in outdoor conditions depending on several variables. The most explanatory parameters we have found are the module temperature, the atmospheric clearness index and the solar spectral irradiance distribution; this latter has been included in the characterization using the average photon energy index as it has been identified as a good indicator of the solar spectral irradiance distribution. Moreover, the variance of instantaneous performance ratio for each studied technology has been analyzed. We can conclude that the joint use of all these parameters in contour graphs allows us to better characterize the performance of modules and to reduce the uncertainty observed in previous proposals that only used two of these parameters.

Analysis and characterization of photovoltaic modules of three different thin-film technologies in outdoor conditions

Rafael Moreno-Sáez[a], Mariano Sidrach-de-Cardona[a], Llanos Mora-López[b,*]

[a] *Dpto. de Física Aplicada II, E.U. Politécnica. Universidad de Málaga, Louis Pasteur 35, 29071 Málaga, Spain.*
[b] *Departamento de Lenguajes y Ciencias de la Computación, ETSI Informática Universidad de Málaga. Campus de Teatinos. 29071 Málaga. Spain*

Abstract

The instantaneous performance ratio of thin-film photovoltaic modules of three different technologies is analyzed and characterized using contour graphs for different outdoor conditions. This parameter changes when modules are working in outdoor conditions depending on several variables. The most explanatory parameters we have found are the module temperature, the atmospheric clearness index and the solar spectral irradiance distribution; this latter has been included in the characterization using the average photon energy index as it has been identified as a good indicator of the solar spectral irradiance distribution. Moreover, the variance of instantaneous performance ratio for each studied technology has been analyzed. We can conclude that the joint use of all these parameters in contour graphs allows us to better characterize the performance of modules and to reduce the uncertainty observed in previous proposals that only used two of these parameters.

Keywords: thin film technologies, photovoltaic modules, performance ratio, contour graphs, outdoor conditions

1. Introduction

Predicting the energy that photovoltaic systems will generate is essential for such installations to be integrated in the power grid. This involves knowing the behaviour of the photovoltaic modules in the different climatic conditions to which they will be exposed. One way of characterizing this behaviour is to

*Corresponding author

estimate the performance ratio (PR) that describes the relationship between the actual and theoretical energy outputs of a PV plant. This is independent of location and can be used to compare different PV plants. It measures the deviation from standard operating conditions as it depends on the meteorological conditions.

The performance of photovoltaic modules is primarily influenced by the intensity of radiation received and the module temperature, T_{MOD}, but also by the spectral distribution of solar radiation. This is especially important when dealing with thin film modules, mainly due to their spectral response, [1], [2], [3], which means that they only use a portion of the whole solar spectral irradiance received on their surface. Furthermore, this type of modules has a more remarkable nonlinear behaviour with respect to the irradiance received regarding modules mono and polycrystalline, [4]. Therefore, many studies including some parameter related to the solar spectrum in the modelling of thin-film modules, such as the spectral factor, SF, in [5]. One of the most used is the average photon energy (APE) as it has been identified as a good indicator of the distribution of solar spectral irradiance. According to Moreno-Sáez and Mora-López, [6], there is a two-way relationship between solar spectral irradiance distribution and the value of average photon energy (APE).

Minemoto et al., [7], propose a methodology to link the solar spectrum with the energy produced by a photovoltaic module. The authors use the data obtained in experiments with silicon modules, both amorphous and crystalline, in Japan. Contour graphs are then used to represent the PR values obtained. The same type of representation is used by Yoshida et al., [8]. Four modules of different technologies were characterized in this last paper: multicrystalline Si (mc-Si), a-Si/microcrystalline-Si (tandem), amorphous Si (a-Si) and a-Si/a-SiGe/a-SiGe triple junction (3-stack); they combine the contour graph of PR proposed by Minemoto et al., [9], with estimated irradiance contour graph to obtain energy values.

In Minemoto et al., [10], contour plots of the average PR value and standard deviation were built for c-Si (cristaline silicon), a-Si and tandem a-Si/μc-Si. Contour plots of data points of irradiance were also built with an irradiance range from 0.2 to 1 kW/m^2 as a function of T_{MOD} and APE for a-Si PV module. They conclude that the PR of a c-Si module (cristaline silicon) is determined by the module temperature while for a-Si and tandem a-Si/μc-Si modules is determined by the APE value.

Takey et al., [11], use modules of the four different technologies used in [8]. The influence on the outdoor performance of modules is analyzed in two

different ways: using APE and module temperature and using clearness index and air mass. Radiation information is then used to estimate the output energy obtained. They conclude that the estimated output energy obtained using either of these two procedures is similar.

In all the above mentioned research filter data is performed, so that only data with PR values lower than 200% and with irradiance values higher than 0.2 kW/m2 were used in order to remove the uncertainty.

In all these cases, the calculated PR value refers to the energy produced by the module compared to that produced in standard conditions. In this paper, the definition of an instantaneous value of the performance ratio, PR_t, is proposed as an extension to the well-known performance ratio that is used for long time periods, typically one year. An extension is therefore proposed of the classic PR concept, which is used for the energy evaluation of the whole system. This PR instantaneous value compares the power value of the module with respect to the power module in standard conditions at a particular moment. Several meteorological and installation parameters have been used to analyze and characterize the PR_t. We propose to use jointly module temperature, APE and clearness index for to obtain a contour graphs of PR_t that integrate all three as we have checked that all these variables are significant. Once analyzed and characterized, this new parameter can be used to establish the real time operation of an installation under certain meteorological conditions.

The rest of the paper is organized as follows. Materials and methods, including data used, are described in Section 2. The proposed methodology to estimate the PR_t of modules is presented in third section. The data used for the experimentation are described in the fourth section. The results obtained are presented and discussed in the fifth section. Finally, the conclusions are summarized in the last section.

2. Materials and methods

2.1. Performance ratio

The performance ratio (PR) is one of the indexes that has been used to evaluate the performance of photovoltaic modules for long periods, typically one year. The PR is defined in IEC61724, [12], in terms of energy yield in a given period of time, and considering the whole system. This parameter gives the overall losses of the PV system related to the expected energy delivered in standard conditions. As an extension of this index, the instantaneous PR is defined as the ratio of the output power of the PV module power normalized

to its peak and global solar irradiance received at the module normalized by the global solar irradiance at standard conditions according to Eq.1:

$$PR_t = \frac{P_{OUT}/P_{STC}}{G/G_{STC}} \quad (1)$$

where:
P_{OUT}, is the maximum power point (W) of the module,
P_{STC}, is the peak power of the module measured at standard conditions (W) and
G, is the global solar irradiance received in the surface of the module (W/m^2),
G_{STC}, is the value of global solar irradiance at standard conditions (1000W/m^2).

The PR_t is dimensionless. Different values of PR_t represent the different working conditions of the module produced by changes in irradiance, air mass, module temperature and spectral distribution of the incident radiation. The PR_t thus indicate the losses or gains relative to their instantaneous power in standard conditions.

2.2. Clearness index

The atmospheric clearness index is defined as the ratio of the solar global irradiance received in a surface and the extraterrestrial radiation, according to the Eq. 2:

$$k_t = \frac{G_t}{G_0} \quad (2)$$

where G_t, is the solar global irradiance received in a horizontal surface and G_0 is the extraterrestrial solar irradiance.

The clearness index represents the overcast conditions and, to some extent, gives an idea of the composition of the atmosphere, the amount of water vapour and aerosols in suspension in the environment that are the main filtration agent of spectral irradiance, [13].

2.3. Average photon energy

A parameter used to characterize the spectral distribution of solar radiation is the average photon energy (APE). The integral of the irradiance across the whole spectrum is divided by the photon flux in order to calculate the APE value, [14] [7], according to the Eq. 3.

$$APE = \frac{\int_a^b E(\lambda)d\lambda}{q \cdot \int_a^b \Phi(\lambda)d\lambda} \quad (eV) \tag{3}$$

A value that can be considered as the standard APE value is obtained if these calculations are performed with the standard spectrum AM 1.5. If the entire range of the solar spectrum is used, ranging from 280-4000 nm, the APE value obtained for the standard spectrum is 1.60eV [15] while if the calculation is performed using only the values range between 350 and 1050 nm the APE obtained is 1.88eV. This range is the part of the spectrum where there is greater contribution of energy and that includes the visual (VIS) and near infrared (NIR) range. This latter value is the most often repeated in the literature that uses the parameter APE, mainly due to the high cost of equipment that measure the infrared spectra as it needs InGaAs sensors that are much less common than silicon sensors used to measure the spectrum in the visible and near infrared range [16].

The APE value provides information on the type of light received, as a different APE value will be obtained depending on the composition of the atmosphere, the time of the day or the year. The APE value is also highly influenced by atmospheric agents. These can mainly be divided into two effects, the Rayleigh dispersion and by aerosols [17] and water vapour [18]. The elements that present greater molecular absorption and which, therefore, have a significant effect on the solar light spectrum in the wavelengths between 300 and 2500 nm, are: water vapour (H_20), ozone (O_3), oxygen (0_2), nitrogen oxide (NO_2)and carbon dioxide (CO_2) [19].

The Rayleigh dispersion influences the lowest wavelengths to a greater extent and the water vapor absorbs part of the spectral irradiance in higher wavelengths. An effect that can be appreciated when there are clouds is that they act as a filter for light in the infrared. The windows caused by the water are located at wavelengths of around 730, 820, 930, 1150 and 1450 nm [20].

The characterization of the global solar irradiance spectrum can be performed using the APE value in the [350,1050] nm interval. In line with the conclusions in [6], all the information of the spectra that have an APE value of between 1.79 and 2.1 can be represented using just three types of distribution of the solar spectrum. We find that all the spectra in this range can be grouped into three different clusters. The APE values that delimit the cluster for each spectrum are shown in Eq. 4.

$$Cluster_{APE_i} = \begin{cases} C_1 & \text{if } APE_i \in [1.79 - 1.88[\\ C_2 & \text{if } APE_i \in [1.88 - 1.92[\\ C_3 & \text{if } APE_i \in [1.92 - 2.1] \end{cases} \quad (4)$$

3. Proposed methodology

This paper seeks to construct the PR_t contour graphs of the thin film modules, using the APE value, module temperature and atmospheric clearness index at the same time. The variability of the data of those contour graphs will be tested, using the standard deviation of each of the contour graph values, as opposed to the variability shown when only two of those parameters are used.

In order to first estimate this last variability, the PR_t values were obtained when only using two of those parameters, as proposed in [11], [7], [9], [10] and [8].

On the one hand, using the module temperature values recorded and the estimated clearness index values for each observation, those values were discretized in order to construct the contour graphs of each module. Thus, the interval to which the T_{MOD} value corresponds and the interval to which the k_t values for each pair of values (T^m_{MOD}, k^m_t)) recorded, identified by m, were established. Those two intervals (indexes, (x^m, y^m)) obtained are the ones that determine the group to which the observation belongs and the ones used to calculate the contour graph.

The T_{min} and T_{max} valued recorded were obtained and 60 different intervals were used for the values of the module temperature. Using the T_{min} and T_{max} values, the limits were defined of each of the 60 intervals, used for the module temperature values, as stated in Eq.5:

$$T_{(i)} = \left\{ \; T_{min} + i \qquad \text{for } i = 0, \ldots, T_{max} - T_{min} \right. \quad (5)$$

The minimum and maximum values are 0 and 1 respectively for the clearness index values. 100 intervals were used for this parameter. The limits of each interval were obtained as per with Eq. 6:

$$k_{t(j)} = \left\{ \; 0.0 + j \qquad \text{for } j = 0.01 \ldots 1.00 \right. \quad (6)$$

Once the module temperature intervals and clearness index had been established, depending on the value of the temperature of the module –T^m_{MOD}–

and of the clearness index value $-k_t^m-$ the group to which $-g_{(i)(j)}^m-$ belongs was calculated using the relevant (i) and (j) indexes, according to Eq. 7:

$$g^m = \begin{cases} g_{(i)(j)} & \text{if } T_{MOD}^m \in [T_{(i)}, T_{(i+1)}), \quad i < 70 \qquad \text{AND} \\ & \text{if } k_t^m \in [K_{(j)}, K_{(j+1)}), \quad j < 1.0 \\ g_{(70)(j)} & \text{if } T_{MOD}^m = 70 \qquad \text{AND} \\ & \text{if } k_t^m \in [K_{(j)}, K_{(j+1)}), \quad j < 1.0 \\ g_{(i)(100)} & \text{if } T_{MOD}^m \in [T_{(i)}, T_{(i+1)}), \quad i < 70 \qquad \text{AND} \\ & \text{if } k_t^m = 1.0 \\ g_{(70)(100)} & \text{if } T_{MOD}^m = 70 \qquad \text{AND} \\ & \text{if } k_t^m = 1.0. \end{cases} \tag{7}$$

The PR_t mean values and their standard deviation were calculated for each group $g_{(i)(j)}$. The PR_t mean value of each group was estimated using Eq. 8.

$$\overline{PR}_{(i)(j)} = \frac{\sum_{l=1}^{n_{(i)(j)}} PR_{(i)(j)}^l}{n_{(i)(j)}} \tag{8}$$

where $n_{(i)(j)}$ is the number of observations that there are in group $g_{(i)(j)}$.

On the other hand, the contour graph of each module was also obtained using the APE values and module temperature. The intervals of the temperature values were defined using Expression 5. For the APE values, the minimum and maximum values used were 1.79 y 2.10 respectively. 31 intervals were used for this parameter. The upper limits of each interval were obtained in accordance with Eq. 9:

$$APE_{(j)} = \left\{ \; 1.79 + j \qquad \text{for } j = 0.01 \ldots 0.31 \right. \tag{9}$$

In a similar way to the procedure described to obtain the contour graphs of PR depending on the clearness index and module temperature, for each reading m recorded, depending on the value of the temperature of the module $-T_{MOD}^m-$ and APE $-APE^m-$ the group was calculated to which $-g_{(i)(j)}^m-$ belongs using the relevant (i) and (j) indexes, according to the module temperature interval and to the APE to which its values belongs, respectively according to Eq. 10:

$$g^m = \begin{cases} g_{(i)(j)} & \text{if } T^m_{MOD} \in [T_{(i)}, T_{(i+1)}), \quad i < 70 \quad \text{AND} \\ & \text{if } APE^m \in [APE_{(j)}, APE_{(j+1)}), \quad j < 2.10 \\ g_{(70)(j)} & \text{if } T^m_{MOD} = 70 \quad \text{AND} \\ & \text{if } APE^m \in [APE_{(j)}, APE_{(j+1)}), \quad j < 2.10 \\ g_{(i)(100)} & \text{if } T^m_{MOD} \in [T_{(i)}, T_{(i+1)}), \quad i < 70 \quad \text{AND} \\ & \text{if } APE^m = 2.10 \\ g_{(70)(100)} & \text{if } T^m_{MOD} = 70 \quad \text{AND} \\ & \text{if } APE^m = 2.10. \end{cases} \tag{10}$$

These expressions were used to obtain the contour graphs for each of the modules tested using clearness indexes and module temperatures, on the one hand, and APE values and module temperatures, on the other hand. In order to analyse the variability of the values of each of these contours, the contour graphs were also constructed for the values of the standard deviation of each pair of values (T_{MOD}, k_t) and (T_{MOD}, APE) of the PR_t contours.

Finally, in order to characterize the PR_t values using those three parameters (module temperature, APE and clearness index), the observations were separated into three different clusters using Eq. 4. For each of those clusters, their PR_t contour graphs were obtained using the clearness index and module temperature as variables.

4. Experimental data

This study used three thin film modules (See Table 1), which were in the same structure, with the same tilt and azimuth (Latitude 36.7°N, Longitude 4.5°W, height above sea level 50 m), which meant that they were all working in the same weather conditions.

Technology	**a-Si**	**a-Si/μc-Si**	**CdTe**
η_{STC} (%)	6.3	8.5	10.1
Area (m^2)	0.95	1.49	0.72
Power (Wp)	60	121	72.5
Range SR (nm)	350-750 (1)	400-1000(2)	330-875(1)

Table 1: Main characteristics of the modules used provided by the manufacturer (except for the spectral response, SR), (1) ref.[21] and (2) ref.[22].

Apart from all the readings recorded for the modules, the data were used supplied by a weather station that includes the reading of the global irradiance on the plane of the modules by means of a pyranometer and has PT-100 resistance temperature sensors joined to the back of the modules to read their temperatures. All the parameters needed to characterise the module were recorded by means of a experimental monitoring system developed in this laboratory [23] capable of measuring simultaneously the electrical characteristic I-V curves with up to 100 points, along with the weather variables. Each I-V curve is traced every five minutes throughout the day for each of the technologies used. A water jet was used to periodically clean the surfaces of modules and other devices have to minimise unwanted effects caused by the accumulation of dust on those surfaces.

Following the guidelines of the standard IEC 60904-7, [24], the inlet of the spectroradiometer was fitted to the same structure where all the measurement devices were placed, in a coplanar manner and not exceeding a tilt difference of 2°. All the measurement elements were placed south-facing at a 20° tilt angle. The spectra were also measured during the day. Data was recorded from all the modules from November 2010 to June 2012. Readings were taken from sunset to sunrise. The following were selected from all the parameters recorded:

- Power at the point of maximum power –P_M–,
- Module temperature –T_{MOD}–,
- Global solar irradiance received on the plane of the –G– and
- Solar spectral distribution, used to estimate the APE values.

5. Results

The PR_t contour graphs were obtained for the different thin film modules using the module temperature and the APE value, on the one hand, and the module temperature and the clearness index value, on the other hand, as independent variables. Furthermore, for each group of observations $g_{(i)(j)}$, with $\overline{PR}_{(i)(j)}$ mean value, the standard deviation values, σ, were estimated. Those values allow possible atypical values [25] be located and obtain information on how representative the mean value is. Finally, the PR_t contour graphs were obtained by using the three variables indicated together.

5.1. PR_t contour graphs depending on APE and module temperature

Fig. 1 shows the mean values of the PR_t calculated for the different thin film modules that were studied using the APE value and module temperature and the methodology described in the third section.

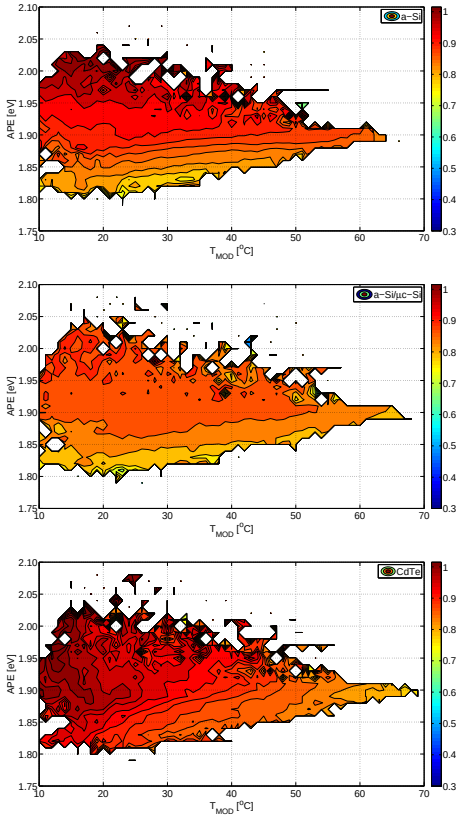

Figure 1: $\overline{PR_t}$ Contour Graphs using the APE and T_{MOD}values, for the modules of the three technologies tested.

In the case of the contour graphs of the **a-Si** technology module (Fig. 1.(a)), the APE value can clearly be seen to have the greatest influence on the PR values, as when that is set, no changes can be seen to the PR values even though the temperature changes; this may be due to other effects that counteract the effect of the increase in temperature, such as thermal annealing effects or seasonal spectral variation, [26]. The greater influence of the APE is due to the reduced bandwidth that the spectral response of the modules of

this technology has. This is also the case, although to a lesser extent, for the a-Si/μc-Si technology module.

In the **microamorphous** technology (Fig. 1.(b)), this type of representation does not contribute a great deal of information as the same PR values are obtained for separate APE values, with the temperature of the module being what conditions the PR values. This is due to the broad bandwidth of the spectral response of this technology absorbing a large part of the spectrum. In this way, the same $\overline{PR}$ value can be obtained for very different APE and module temperature values. For example, when observing Fig. 1.(b) it can be seen that the same PR is obtained for the pair of values ($T_{MOD} = 20^oC, APE = 1,97eV$) as for the pair ($50^oC, 1,90eV$), which again indicates that it is not easy to characterise the operating of modules of this technology [4].

As regards the **CdTe** module, this representation (Fig. 1.(c)) does seem more convenient as different $\overline{PR_t}$ values are obtained as the APE values and the module temperatures change. This module has an intermediate spectral response bandwidth with respect to the other two technologies, so that the spectrum does not condition the operating of the module, as occurs with the a-Si technology studied, but its effect on the performance rate can be seen.

This type of representation using the APE and module temperature variables is only capable of obtaining significant information for one of the analyzed technologies. For this reason it can be concluded that although this procedure is valid for c-Si, [10], it is not a proper procedure for characterizing all thin-film module technologies as we have already stated, no changes can be seen to the PR values even though the temperature changes.

Behaviour that can be appreciated in the three tested technologies is the high PR_t value with high APE values, corresponding to days with low clearness indexes.

5.2. PR_t contour graphs depending on clearness index and module temperature

Fig. 2 shows the mean values of the PR_t calculated for the different thin film modules that are studied using the clearness index and module temperature.

In order to explain the results shown in these graphs, it should be noted that the effect of the water vapour on the spectral distribution of the solar irradiance is important in the low clearness index values. This effect can be seen in a shift of the spectral irradiance to the "blue" so that practically the whole energy contribution is given by the lower wavelengths.

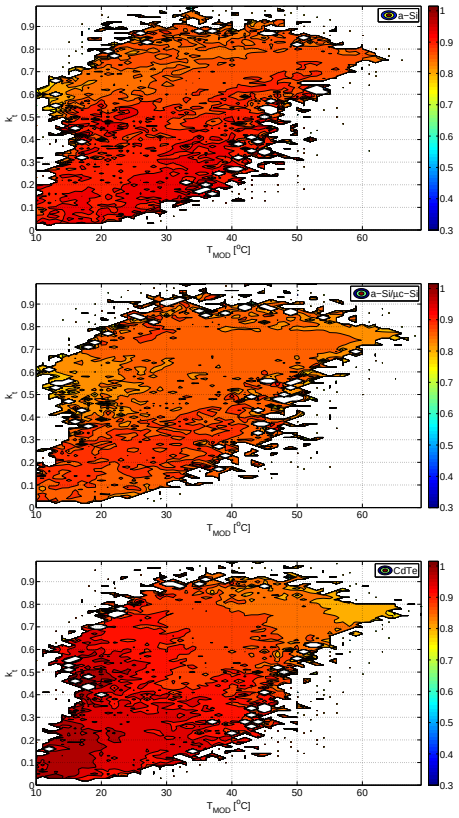

Figure 2: $\overline{PR}$ Contour Graphs using the k_t and T_{MOD}values, for the modules of the three technologies tested.

The dependency of the PR_t on the parameters tested is different for each technology, see Fig. 2. However, there is behaviour that is repeated in all of them: the mean PR of the modules is very high for low module temperatures and with small clearness indexes.

A high PR_t with a low clearness index (under 0.5) means that the whole solar spectrum received is being used by the module as the thin film modules tested capture, above all, the light emitted in this wavelength due to the shorter bandwidth of its spectral response.

The width of the spectral response of the module explains that better PR_t mean values for the CdTe and a-Si module (narrower special response) and lower values of the mean PR_t for the a-Si/μc-Si module.

At least three subgroups related to the value of the clearness index can be

seen using the module temperature and clearness index (Fig. 2).

5.3. PR_t contour graphs depending on APE, clearness index and module temperature

The data was clustered using Eq. 4 in order to include the information on the spectral composition of the solar radiation in the PR_t contour graphs. The PR_t contour graph for each of those clusters was obtained using Eq. 5, 6 and 7 in order to establish the observations that belong to each cluster, and Eq.8 for estimating the mean values of PR_t for each $(T_{MOD}, k_t, cluster_{APE})$.

It was seen that for a same pair of values (T_{MOD}, k_t), the experimental PR_t value is different depending on the APE value (cluster) which appears to indicate that our proposal to use the clusters obtained in [6] to represent the information of the spectral composition (using the APE value) may be adequate. For example, in Table 2, (a-Si module), it can be observed that for $T_{MOD} = 25°$ and $k_t = 0.4$, the PR_t values of 0.89, 0.94 and 0.93 are obtained for each of the clusters, which shows that effectively the spectrum in each of those clusters is different.

		Module Temperature (°C)						
		22	**23**	**24**	**25**	**26**	**27**	**28**
Clearness Index 0.39	*Cluster*1	0.84	0.85	–	0.82	0.78	0.89	–
	*Cluster*2	0.93	0.94	0.93	0.88	0.96	0.92	0.91
	*Cluster*3	0.95	0.96	0.93	0.98	0.92	–	0.93
0.40	*Cluster*1	–	–	0.88	0.89	0.85	0.83	0.84
	*Cluster*2	0.91	0.90	0.88	0.94	0.91	0.93	0.93
	*Cluster*3	0.00	–	–	0.93	–	0.95	0.98
0.41	*Cluster*1	0.86	0.97	0.83	0.94	0.83	–	0.77
	*Cluster*2	0.89	0.89	0.89	0.88	0.91	0.89	0.89
	*Cluster*3	0.94	–	–	0.93	0.99	0.98	0.97

Table 2: Contingency table of the PR_t values according to T_{MOD} and k_t and APE value interval (as per to those defined for each cluster).

The results obtained for each of the technologies tested are set out and discussed in the following sections.

5.3.1. a-Si technology

Fig. 3 shows the results obtained for the mean PR_t values in each analyzed cluster for a-Si module using the module temperature value and the clearness

index.

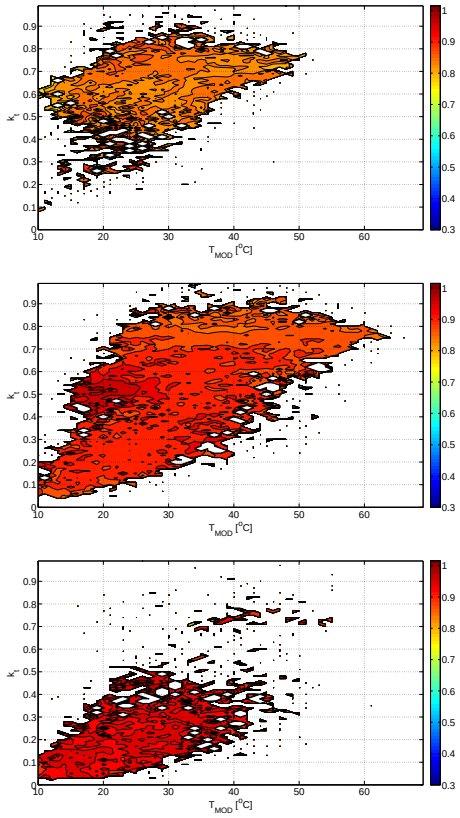

Figure 3: $\overline{PR}$ of a-Si module in each cluster

When the module is working in the first cluster, corresponding to clear days (the spectrum of the solar light shifts to the "red") the $\overline{PR_t}$ of the module is not very high. It ranges between 0.75 and 0.90 (Fig. 3.(a)), as it is not capable of capturing the spectral irradiances that are in the infrared due to the spectral response of the module. The $\overline{PR_t}$ value is under 1, even at temperatures under 25 °C.

In the figure for the second cluster, Fig. 3.(b), it can be seen that the $\overline{PR_t}$ increases due to the module capturing increasingly more energy from the incident spectrum; this is because as the spectrum shifts to the "blue", the atmosphere has more suspended water vapour and the high wavelengths begin to be filtered. It can be seen how, when the clearness k_t drops from 0.7, the PR_t increases and remains practically constant. This indicates that it increases

the contribution of the wavelengths that are in the same spectral range as the spectral response of the module. This behaviour is confirmed when only the mean PR_t corresponding to very high APE values, third cluster (Fig. 3.(c)), is represented. The proportion of the solar spectrum that the module captures is maximum, that is, the incident spectrum is the one that most coincides with its spectral response.

None of the contour graphs presented for this technology shows a significant variation of the PR_t values with the operating temperature of the modules; this can be explained because PR_t variations due to changes in the spectrum are compensated by other effects, as mentioned above, section 5.1.

5.3.2. a-Si/μc-Si technology

Fig. 4 shows the mean performance ratio in each analyzed cluster for a-Si/μc-Si module using the module temperature value and the clearness index.

Different $\overline{PR_t}$ values have also been obtained in this module according to the APE (cluster), for a single temperature value and atmospheric clearness index.

In this technology, the range of wavelengths that the module is capable of capturing (VIS+NIR) is just over 1000 nm. Therefore, the $\overline{PR_t}$ values obtained in practically all the cluster is more uniform in the different conditions compared to those obtained by other technologies, see Fig. 4.

If the contour graphs are analysed according to the different APE values, in the first cluster, with shift to the "red" (Fig. 4.(a)), it can be seen that the module provides a $\overline{PR_t}$ over 0.9 with a clearness index over 0.7 and working temperature of around the standard operating conditions.

In the second cluster, where the majority of the spectra are found, the temperature of the module is the determining factor on the PR_t, as has already been noted by other authors, see [13]. The performance rate falls for high module temperature and this $\overline{PR_t}$ increase for low ones, see Fig. 4.(b).

In the third cluster, with the majority of the spectra in the "blue" zone, the majority of the $\overline{PR_t}$ values obtained are over 0.95 for any operating temperature, Fig. 4.(c). This is due to the incident spectrum being adequate for the spectral response of the cell and the temperature of the modules has little influence.

This technology clearly shows that having a spectral response with a broad bandwidth, the spectral variations will not affect the a-Si/μc-Si modules, as it will be capable of capturing light both at high and low wavelengths.

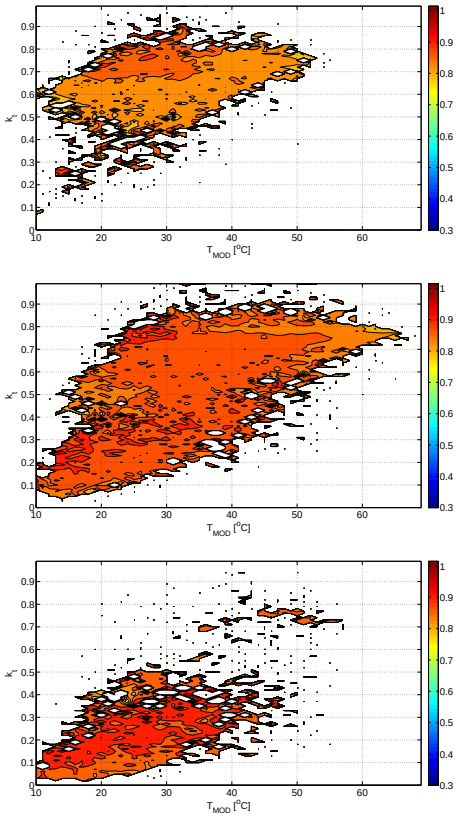

Figure 4: $\overline{PR_t}$ of a-Si/μc-Si module in each cluster.

5.3.3. CdTe technology

The $\overline{PR_t}$ results according to the clusters for the CdTe module are shown in the contour graphs in Fig. 5 using the module temperature and the clearness index.

Those results show that the module performance is influenced both by the clearness index and by the module temperature, see Fig. 2.(c). As in the same way as in the two previous technologies, the effect explained in Table 2, the different $\overline{PR_t}$ values according to the cluster for the same temperature and clearness index values can be seen.

When only the $\overline{PR_t}$ values of the spectral irradiances that are found in the first cluster are used, see Fig. 5.(a), the performance of the modules is mainly determined by the working temperature of the module, as those values indicated that the spectrum has shifted to the "red" and the spectral response

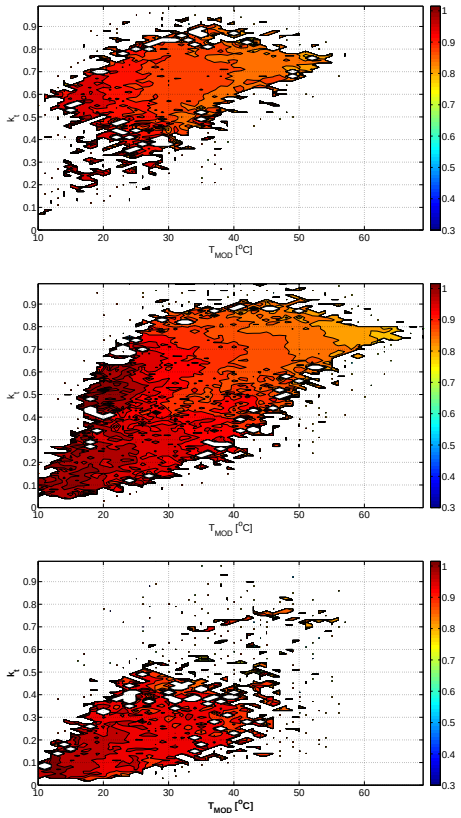

Figure 5: $\overline{PR_t}$ of CdTe module in each cluster

of the device does not manage to capture much of the energy received.

In the second cluster, Fig. 5.(b), it can be seen that the effect of the temperature of the module is very decisive, but an influence of the spectral distribution can be seen. In the case of low clearness index, the greatest spectral contribution will come from the low wavelengths, which is where the spectral response of this module is found. This, together with the fact that a high module temperature is not generally reached on those days, means that the performance rate attains a high value.

The $\overline{PR_t}$ calculated in the third cluster are very high. This is because, in general, the observations of this cluster correspond to small values of the clearness index, corresponding to spectral distributions in the spectral response range of the module. This behaviour can be clearly seen in Fig. 5.(c).

5.4. Analysis of the variability of the different representations

The standard deviation calculated for each pair of values is significant at some points of the contour graphs of the three proposed representations. That means that significantly different PR_t values were obtained for the same module temperature and clearness index conditions, or same module temperature and APE values conditions, or same conditions of the three parameters.

A study of their variability was performed, using the standard deviation observed for each pixel of each contour graph, to compare these representations and analyse the precision of each of them.

Once the standard deviation values of the points of each contour graph were calculated, the accumulated distribution of those values was calculated. Table 3 presents the results obtained for each type of contour graph and technology. These values provide an indication of the dispersion that the PR_t values have for each point in each contour graph.

% of STD values	**a-Si**			**a-Si/μc-Si**			**CdTe**		
	Tmod vs			Tmod vs			Tmod vs		
less than	APE	Kt	APE-Kt	APE	Kt	APE-Kt	APE	Kt	APE-Kt
0.01	20.2	18.8	32.8	20.9	20.1	34.6	17.7	20.8	35.5
0.02	29.7	28.3	46.2	33.6	33.5	53.4	29.5	35.2	50.1
0.03	50.8	46.3	65.7	62.1	60.4	76.1	47.9	54.6	69.9
0.04	78.5	66.2	83.3	79.9	80.1	88.2	70.6	74.3	84.1
0.05	91.2	80.4	92.0	88.3	88.7	93.2	85.0	87.0	92.5
0.06	95.3	88.9	95.9	91.6	93.2	95.8	92.4	94.0	96.0
0.07	97.0	93.5	97.4	94.5	95.0	97.0	95.4	96.3	97.5
0.08	97.7	96.7	98.4	95.9	96.2	97.6	96.6	97.4	98.4
0.09	98.2	98.0	98.8	96.5	97.4	98.3	97.7	98.1	98.8
0.10	98.5	98.6	99.0	97.1	97.9	98.7	98.4	98.6	99.0

Table 3: Cumulative distribution of values of standard deviation (STD) (%)

For the three technologies tested, it can be seen that contour graphs obtained using the module temperature, clearness index and cluster of APE have the lowest values of standard deviation that means this representation allows to better estimate the PR_t of modules; over 90% of the PR_t values were estimated with a standard deviation under 0.05.

For the other two types of representation, a contour graph using module temperature and APE is more accurate (less standard deviation) for a-Si technology whilethat using module temperature and clearness index is better for CdTe technology. In the case of a-Si/μc-Si technology, both representations

achieve similar standard deviation values that agrees with previous results obtained by [11].

6. Conclusions

A methodology to characterize the operating of photovoltaic modules using different thin film technologies for real conditions has been proposed. This methodology has obtained the contour graphs that allow the instantaneous performance ratio for those modules to be established. The aim was to obtain contour graphs according to the parameters that are most significant in the operating of those modules, which include the clearness index, the working temperature of the module and the APE value. This last value can be estimated using several meteorological parameters.

The operating of three different thin film modules technology has been tested in detail and the effect of the spectral distribution of the irradiance on that has been checked.

Using contour graphs representing the operating of the photovoltaic modules through the instantaneous performace ratio clearly provides a large amount of information on thin film technologies and provides us with real-time information on how modules of analyzed modules are operating as these curves allow the performance rate of the modules in real operating conditions to be estimated. The standard deviation values of the performance rate at each point were also estimated for each of these contour graphs. This allows the accuracy of the predictions to be checked.

The accuracy of two of the proposed representations is similar, as has been pointed out by [11]; nevertheless in both cases the variability of PR_t estimates is significant for some values of these parameters. Taking into account these results, we have proposed a procedure that allows to use jointly these three variables for estimating the PR_t. It is based on previous results presented in [6] that establish that all spectral distributions of solar radiation and therefore APE values can be represented only using 3 different curves, characterized by three different APE ranges. We have estimated the contour graphs using these three parameters. These graphs are more accurate that previously obtained only using two of these parameters. These contour graphs could be used jointly with irradiance global data in future research to estimate the energy generated by PV modules, [11].

Acknowledgments

This research has been partially supported by the Spanish Consejería de Economía, Innovación y Ciencia of the Junta de Andalucia under projects P10-TIC-6441 and P11-RNM-07115.

[1] N. Martín and J. M. Ruíz. A new method for the spectral characterization of pv modules. *Prog. Photovolt: Res. Appl.*, 7:299–310, 1999.

[2] C. Monokroussos, M. Bliss, Y.N. Qui, C.J. Hibberd, T.R. Betts, A.N. Tiwari, and R. Gottschalg. Effects of spectrum on the power rating of amorphous silicon photovoltaic devices. *Prog. Photovolt: Res. Appl.*, 19:640–648, 2011.

[3] Tetsuyuki Ishii, Kenji Otani, Takumi Takashima, and Yanqun Xue. Solar spectral influence on the performance of photovoltaic (pv) modules under fine weather and cloudy weather conditions. *Prog. Photovolt: Res. Appl.*, 21(4):481–489, 2011.

[4] IEC.60904-8. *CEI/IEC 60904-8 ed2.0: Photovoltaic devices. Part 8, Measurement of Spectral Response of a Photovoltaic (PV) Device*. International Electrotechnical Commission: IEC technical committee 82: Solar photovoltaic energy systems, 1998.

[5] G.Nofuentes, B. Garcia-Domingo, J.V.Munoz, and F.Chenlo. Analysis of the dependence of the spectral factor of some pv technologies on the solar spectrum distribution. *Applied Energy*, 113:302–309, 2014.

[6] Rafael Moreno-Sáez and Llanos Mora-López. Modelling the distribution of solar spectral irradiance using data mining techniques. *Environmental Modelling & Software*, 53(0):163–172, 2014.

[7] Takashi Minemoto, Shingo Nagae, and Hideyuki Takakura. Impact of spectral irradiance distribution and temperature on the outdoor performance of amorphous si photovoltaic modules. *Solar Energy Materials & Solar Cells*, 91(10):919–923, 2007.

[8] Shota Yoshida, Seiya Ueno, Naoya Kataoka, Hideyuki Takakura, and Takashi Minemoto. Estimation of global tilted irradiance and output energy using meteorological data and performance of photovoltaic modules. *Solar Energy*, 93(0):90–99, 2013.

[9] Takashi Minemoto, Shunichi Fukushige, and Hideyuki Takakura. Difference in the outdoor performance of bulk and thin-film silicon-based photovoltaic modules. *Solar Energy Materials & Solar Cells*, 93:1962–1965, 2009.

[10] Takashi Minemoto, Hiroaki Takahashi, Yasuhito Nakada, and Hideyuki Takakura. Outdoor performance evaluation of photovoltaic modules using contour plots. *Current Applied Physics*, 10(2, Supplement):S257–S260, 2010. The Proceeding of the International Renewable Energy Conference and Exhibition 2008 (RE2008) The Proceeding of the International Renewable Energy Conference and Exhibition 2008 (RE2008).

[11] Ryosuke Takei, Takashi Minemoto, Shota Yoshida, and Hideyuki Takakura. Output energy estimation of si-based photovoltaic modules using clearness index and air mass. *Japanese Journal of Applied Physics*, 51(10S):10NF10 1–10NF10 5, 2012.

[12] IEC61724. *IEC 61724, Photovoltaic system performance monitoring. Guidelines for measurement, data exchange and analysis*. CENELEC, 2000.

[13] Yasuhito Nakada, Hiroaki Takahashi, Kyoko Ichida, Takashi Minemoto, and Hideyuki Takakura. Influence of clearness index and air mass on sunlight and outdoor performance of photovoltaic modules. *Current Applied Physics*, 10:261–264, 2010.

[14] S. R. Williams, T.R. Betts, T. Helf, R. Gottschalg, H.G. Beyer, and D.G. Infield. Modelling long-term module performance based on realistic reporting conditions with consideration to spectral effects. In *Photovoltaic Energy Conversion, 2003. Proceedings of 3rd World Conference on*, volume 2, pages 1908–1911 Vol.2, 2003.

[15] T.R. Betts, R. Gottschalg, and D.G. Infield. *Spectral Irradiance Correction For PV System Yield Calculations*. 19th European Photovoltaic Solar Energy Conference, 2004.

[16] Cristina Cornaro and Angelo Andreotti. Influence of average photon energy index on solar irradiance characteristics and outdoor performance of photovoltaic modules. *Prog. Photovolt: Res. Appl.*, 21(5):996–1003, 2013.

[17] C. P. Jacovides, Michael D. Steven, and D. N. Asimakopoulos. Solar spectral irradiance under clear skies around a major metropolitan area. *J. Appl. Meteor.*, 39(6):917–930, June 1999.

[18] C. Riordan, R. Hulstrom, T. Cannon, D. Myers, and T. Stoffel. Photovoltaic advanced research and development project: Solar radiation research annual report. Technical report, Solar Energy Research Institute, 1617 Cole Boulevard Golden, Colorado 80401-3393, 1990.

[19] R.E. Bird, R.L. Hulstrom, and L.J. Lewis. Terrestrial solar spectral data sets. *Solar Energy*, 30(6):563 – 573, 1983.

[20] Stefan Nann and Carol Riordan. Solar spectral irradiance under clear and cloudy skies: Measurements and a semiempirical model. *J. Appl. Meteor.*, 30(4):447–462, 1991.

[21] F. Pérez-López, J. J.and Fabero and F. Chenlo. Experimental solar spectral irradiance until 2500 nm: Results and influence on the pv conversion of different materials. *Prog. Photovolt: Res. Appl.*, 15:303–315, 2007.

[22] Holger Seifert, Jochen Hohl-Ebinger, and Wilhelm Warta. Spectral influences on measurement uncertainty of a-si/μc-si multi-junction solar devices. In *26th European Photovoltaic Solar Energy Conference and Exhibition*, pages 2714–2717, 2011.

[23] M. Piliougine, J.E. Carretero Rubio, Mora Lopez L., and M. Sidrach de Cardona Ortin. Experimental system for current-voltage curve measurement of photovoltaic modules under outdoor conditions. *Progress in Photovoltaics*, pages 1–12, 2011.

[24] IEC.60904-7. *CEI/IEC 60904-7 ed3.0: Photovoltaic devices. Part 7, Computation of the spectral mismatch correction for measurements of photovoltaic devices*. International Electrotechnical Commission, IEC technical committee 82: Solar photovoltaic energy systems, 2008.

[25] Neil D. Bennett, Barry F.W. Croke, Giorgio Guariso, Joseph H.A. Guillaume, Serena H. Hamilton, Anthony J. Jakeman, Stefano Marsili-Libelli, Lachlan T.H. Newham, John P. Norton, Charles Perrin, Suzanne A. Pierce, Barbara Robson, Ralf Seppelt, Alexey A. Voinov, Brian D. Fath, and Vazken Andreassian. Characterising performance of environmental models. *Environmental Modelling & Software*, 40(0):1 – 20, 2013.

[26] Tetsuyuki Ishii, Kenji Otani, Takumi Takashima, and Kazuaki Ikeda. Change in i-v characteristics of thin-film photovoltaic (pv) modules induced by light soaking and thermal annealing effects. *Prog. Photovolt: Res. Appl.*, 22:949–957, 2014.